Behavioural Patterns of Fine Sands

V.N. Georgiannou[1]
[1]*Department of Civil Engineering, National Technical University of Athens, Greece*
E-mail: vngeor@civil.ntua.gr

ABSTRACT: The behavioural patterns of five fine sands are investigated in the Hollow Cylinder and the triaxial apparatus under undrained loading conditions. The paper focuses on distinctive patterns of undrained response of sands, namely an unstable or brittle response associated with strength reduction after a transient peak and a stable response when a continuous increase in strength with loading is observed. The influence of various parameters such as particle shape, grading, addition of fines, consolidation history, stress level and loading conditions on sand behaviour is examined. Particle shape and angularity has much more significant influence on a sand's response pattern than small variations in the grading curves of uniform sands. However, larger variations in the grading curves or the addition of even small contents of fines (<5%) can also alter the behaviour of a sand from stable to brittle. The response of a sand to cyclic loading is related to its response to monotonic loading. Anisotropic consolidation does not appear to alter the mobilized angle at failure and phase transformation during torsional loading.

1. INTRODUCTION

The behaviour of sands under monotonic and cyclic loading has been the subject of various studies in the past, with emphasis placed on instability of loose sands under undrained loading conditions. Key parameters such as density, method of specimen formation in relation to the produced fabric, consolidation history, confining stress, type of loading (monotonic or cyclic, loading direction, with or without principal stress rotation), loading mode (load or deformation controlled), presence of fines that affect the behaviour of a sand have been identified and reported widely. These studies have enabled a better understanding of the parameters controlling the behaviour of sands. The range of these parameters though reflects the complexity of the problem.

Testing of homogeneous (uniform) specimens under uniform states of stress and strain is required for fundamental studies of sand behaviour. Apart from uniform and repeatable specimens certain stringent experimental requirements need to be met in order to isolate the influence of one parameter on the response of a sand. In the present study an experimental investigation is presented to provide evidence useful to obtain a better understanding of sand behaviour.

The primary objective of this paper is to establish, experimentally, the stress-strain response of five fine sands and identify the key parameters that affect the patterns of their response, namely stable (continuous increase in shear stress) or unstable (decrease in shear stress after a transient peak). Conscious efforts were made in this study to use the same preparation method, testing techniques and void ratio and/or relative density throughout the testing program to facilitate comparison of sand behaviour to undrained loading in the hollow cylinder and the triaxial apparatus.

The effect of the following was investigated: particle shape and angularity, the addition of small fines contents, method of loading application (load-deformation control), monotonic versus cyclic loading and isotropic versus anisotropic consolidation. The study was mainly concentrated on loose to medium dense specimens prepared by water pluviation. Pluviation is considered to create a grain structure that duplicates closely the anisotropy observed in naturally deposited sands [1]. On the other hand, in nature, a given depositional process will produce different densities depending on the gradation of the soil. Since the sands investigated in this study have similar gradations the 'loosest' initial states resulting from the same depositional method, namely pluviation, were of similar density and this formed the basis of comparison of the patterns of behaviour of the sands.

Unstable behaviour and/or liquefaction of sand is often considered as a triggering factor for the failure of loose granular slopes. It has to be mentioned that contractive soils may not always catastrophically fail but may show a range of deformations and instability is not synonymous with failure [2], [3]. It has been recognized from a number of laboratory tests that contractant (loose) sand specimens under undrained monotonic loading show unstable behaviour and drop (temporary or permanent) in shear stress after peak (transient) ([4], [5], [6], [2], [7], [8]). Instability behaviour of sand has been observed under drained loading conditions [9], [10] and under load controlled loading mode [11]. One of the aims of this paper is to examine the factors that affect the 'fabric' (arrangement of particles) of a sand and introduce unstable behaviour.

2. MATERIALS AND TESTING METHODS

2.1 Materials

The materials employed in this study were five fine grained sands, the Ham River sand (HRS) [12], the Fontainebleau sand (FS), the M31 sand (M31), the Longstone sand (LS) and Jamuna sand (JS).

Table1 Minimum and maximum values of void ratio and specific gravity for the sands

	HRS	FS	M31	LS	JS
G_s	2.66	2.64	2.65	2.64	2.65
e_{min}	0.526	0.540	0.528	0.614	0.537
e_{max}	0.870	0.865	0.870	0.995	0.885

The Longstone sand, which consists of fine angular grains, exhibits larger values of e_{min}=0.614 and e_{max}=0.995 compared to the other sands also included in Table 1 together specific gravity values. The grain size distribution curves for all sands are given in Fig. 1.

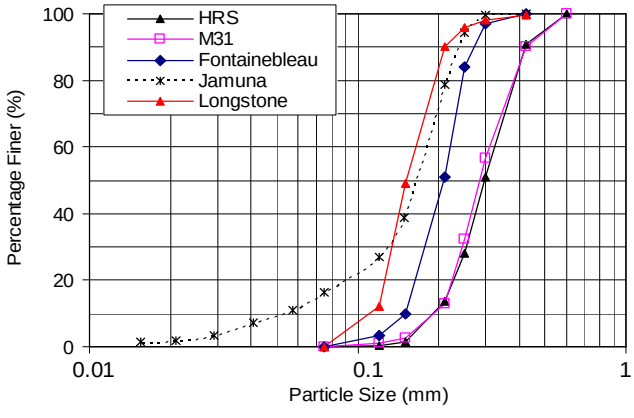

Figure 1 Grading curves

HRS and Jamuna sand have been mixed with platy muscovite mica particles and silt at various contents. Mica MF60, is of comparable grain size to Jamuna sand and is referred to as sand-size mica (m). The average sand-size mica flake has an aspect ratio of about 50. Additionally, very fine mica SX powder (referred to as silt-size mica, sxm) and HPF4 silt [13], were employed to gain comparative results. The grading envelopes for the added materials are shown in Fig. 2.

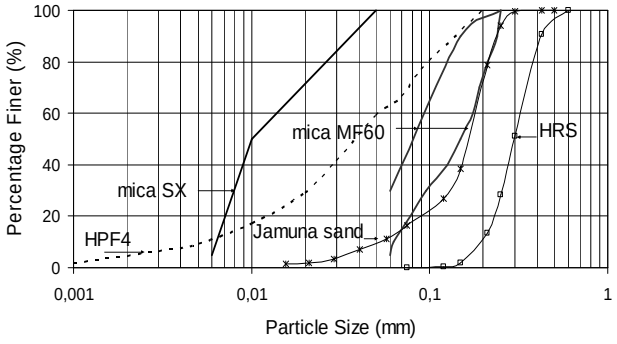

Figure 2 Grading curves of added materials

2.2 Apparata and testing methods

Most of the tests in this study were performed in the hollow cylinder apparatus of the National Technical University of Athens. A detailed description of the hollow cylinder apparatus has been given elsewhere [14]. Axial displacement is measured externally and twist is measured inside the cell at the top platen using a miniature rotary position sensor. Axial load and torque are both measured internally.

All the tests were performed by keeping the same internal and external pressure (p_i=p_o) resulting in b = $\sin^2\alpha$, where the parameter $b = (\sigma_2 - \sigma_3) / (\sigma_1 - \sigma_3)$ expresses the influence of the intermediate stress σ_2 on soil response and α is the angle of σ_1 with the vertical direction. Torsional loading was applied under stress control and the axial load was kept close to zero during testing so that the angle α was equal to 45^o soon after the beginning of shearing. Cyclic tests were performed at a frequency of 0.1Hz.

Tests were controlled and interpreted in terms of average stresses and strains according to the equations, suggested by Hight et al. (1983) [15]. The average shear stress and shear strain are defined by Eqs. (1), where r_o and r_i are the current inner and outer

$$\tau_{\theta Z} = \frac{3M_T}{2\pi(r_0^3 - r_i^3)} \qquad \gamma_{\theta Z} = \frac{2\theta(r_0^3 - r_i^3)\vartheta}{3H(r_0^2 - r_i^2)} \tag{1}$$

radii, M_T the applied torque, θ the circumferential angular displacement and H the initial height of the specimen. The specimens had an outer diameter of 70mm, an inner diameter of 40mm and a height of approximately 140mm.

Additional tests were performed in computer-controlled hydraulic triaxial cells [16]. The overall stability of the system results in a scatter of ±0.1kPa and ±0.1N in the measurements of cell and pore water pressures and axial load, respectively. Pairs of electrolytic level strain gauges of the type described in [17] and submersible LVDTs were mounted diametrically opposite over a central gauge length of the specimen to measure local axial displacements. Triaxial tests were performed on 38mm diameter cylindrical specimens with height to diameter ratio of 2:1. Axial stresses were applied through rough ends.

Anisotropically consolidated specimens followed initially a constant σ_r' drained stress path, from a mean effective stress s'=20kPa up to the line of constant stress ratio k= σ_r'/ σ_a'=0.49, and then followed the constant stress ratio line. Tests at higher pressures were performed in a triaxial apparatus with maximum cell pressure of 7Mpa and maximum axial load 50kN. The stability of the system for cell pressures up to 4MPa is 0.5kPa. Triaxial tests were performed under stress and strain control.

2.3 Formation of specimens

All specimens tested in the hollow cylinder apparatus were formed by pluviation through water [15], [18], a method which produces specimens that simulate naturally deposited sands [19], [1]. The soil fills the split mould falling from a constant height. The relative density of the specimens after consolidation and prior to shearing was Dr=40±2%. Denser specimens were obtained by tapping the mould of the specimen after the sand had settled through the water.

After confirming saturation, with B values in excess of 0.97, specimens were isotropically consolidated to a range of effective stresses, $p_c' = (\sigma_1' + \sigma_2' + \sigma_3')/3$. An ageing period of 12 hours preceded shearing. Water pluviation was also used for the preparation of all clean sand specimens tested in the triaxial apparatus.

For the various mixtures of clean sands with fines air pluviation was used for the formation of the specimens. In the air the drag is less than in water and the fall velocity is higher so the particle orientation should be more random and particle segregation reduced. Prior to placing the dry soil in the funnel dry sand and mica or silt, which had been previously weighed, were thoroughly mixed within a graduated cylinder by turning it upside down and back again until a consistent texture could be observed by naked eye, and this required 4-5 turns of the cylinder. A suction of 20kPa was applied after placing the top cap on the specimen and was maintained throughout the saturation period. Saturation of the specimens was attained by flushing them with carbon dioxide for a period of 30min, after which de-aired water was slowly percolated from the bottom up through the top of the specimens.

3. EXPERIMENTAL RESULTS

3.1 Effect of grain shape

Four out of the five sands shown in Fig. 1, all formed by the same method of pluviation and subjected to the same testing techniques, are sheared in the hollow cylinder apparatus and show markedly different response to undrained loading at similar void ratios in a loose state. Specimen characteristics are shown in Table 2. The response of a sand was categorised as stable when a continuous increase in shear stress with loading is observed and unstable or brittle when shear stress reduces with loading after a transient peak. Unstable behaviour was not associated with collapse since specimens exhibited dilative tendencies after phase transformation. This huge variation in response is observed despite the fact that the four sands are fine and uniform quartz sands with D50=0.15-0.29mm. Furthermore, to eliminate the effect of grading, two sands with identical grading, HRS and M31, are compared first in Fig. 3. Apart from same preparation procedures the sands share similar void ratios at the end of consolidation e=0.728 - 0.735 or D_r=39.3% - 41.3% for HRS (tests HRS_1-4 in Table 2) and e=0.731-0.733 or D_r=40.1% – 40.6% (tests M31_1-3 in Table 2).

In Fig. 3 the two distinctive patterns of behaviour can be observed. HRS (Fig. 3(a) and (d)) shows continuous increase in strength with torsional shear while M31 shows brittle response in Figs 3(b) and (d) where the undrained stress paths and stress-strain curves are shown respectively. The excess pore water pressures shown in Fig. 3(c) indicate dilative tendencies after phase transformation for both sands. The phase transformation points have been marked by solid and broken arrows in Fig. 3(c) for HRS and M31 sand respectively. The application of torsional load is stress controlled. As a result the part of the stress paths in Fig. 3(b) between trancient peak and phase transformation is followed within approximately a second, while data was recorded at six readings per second. Under torsional loading the two sands have similar angles of shearing resistance $\varphi' = 36^0$ and 38^0 and phase transformation angles $\varphi'_{PTL} = 30^0$ and 31^0. For M31which shows brittle response the instability line (IL), proposed by Lade (1993) [2], which joins

(a)

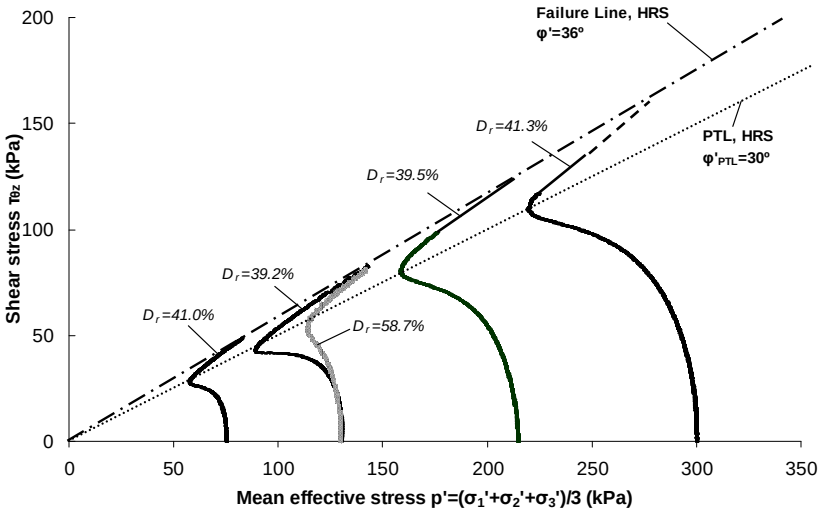

(b)

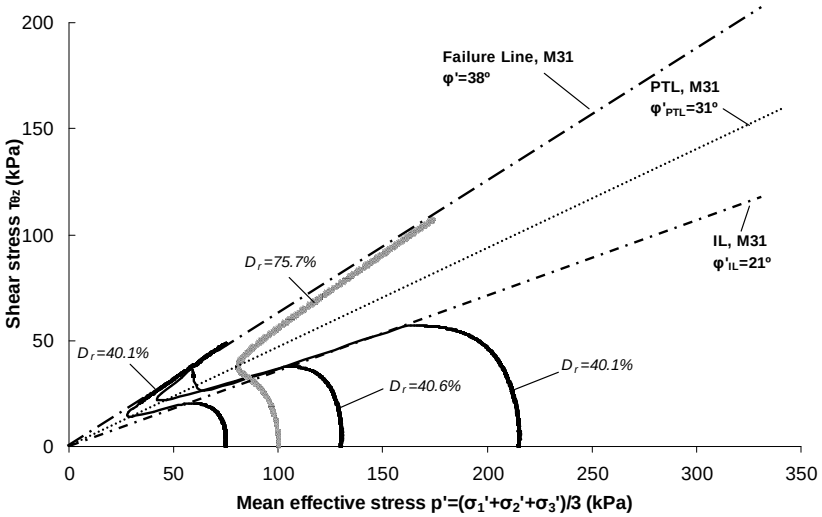

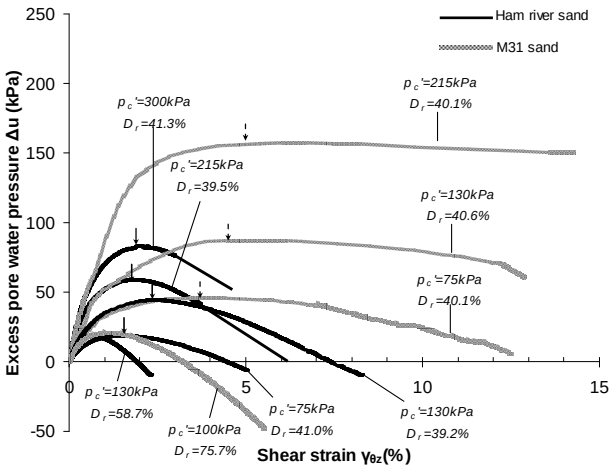

(c)

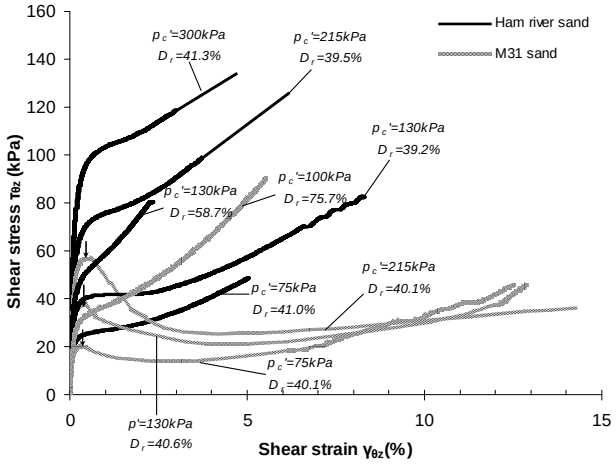

(d)

Figure 3 Torsional shear tests: (a) effective stress paths, HRS; (b) effective stress paths, M31 sand; (c) excess pore water pressure against shear strain curves for both sands; (d) stress-strain curves for both sands

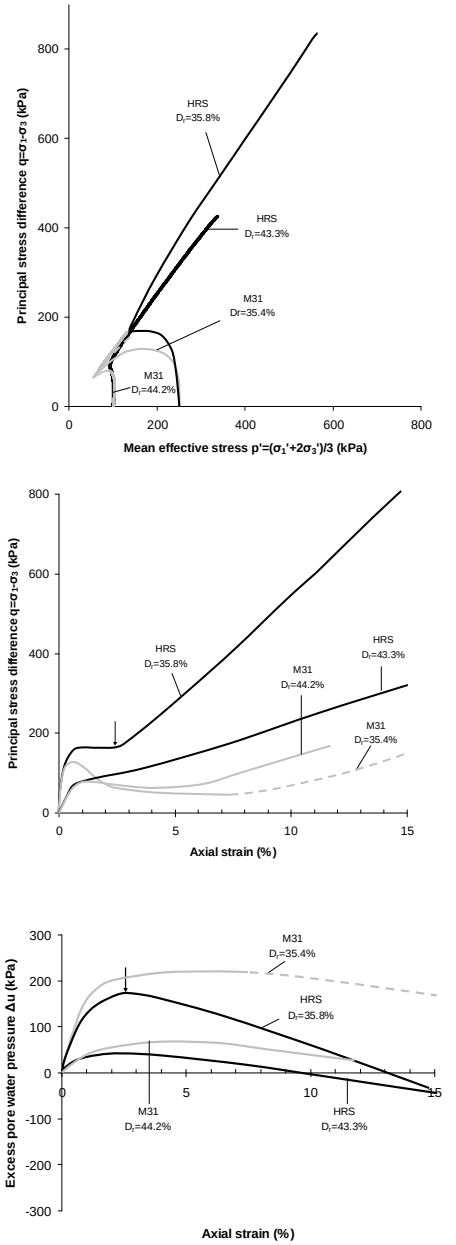

Figure 4 Comparison of the response to undrained triaxial compression of HRS and M31 sand

the transient peak points of the effective stress paths and the origin of the stress space has been plotted in Fig. 3(b) and the mobilized angle, $\varphi'_{IL}=21^0$, was determined.

Finally, a denser specimen (M31_4, Dr=75.7%) has been included in Fig 3. At this density brittleness is suppressed and the response of the sand shows contractive tendencies but it is stable. A denser specimen of HRS included in Fig. 3 also shows suppressed contractive tendencies. The same observations regarding the respective behaviour (stable or brittle) of the two sands are made under triaxial stress controlled loading conditions as shown in Fig. 4. Comparison is made at similar void ratios covering loose and medium density specimens, as indicated in Table 2 where the specimen characteristics are shown (HRS_6, 7 and M31_5, 6). In either case HRS continues gaining strength with loading while M31 sand shows brittle response.

Figs 5 and 6 show the shape and surface of the grains for all sands considered in this paper. Visual inspection of the grains of the sands under the electron scanning microscope in Fig. 5 shows that Longstone and Jamuna sands have clearly angular particles while M31 and Fontainebleau sands, shown in Fig. 6, have rounded to subrounded grains according to Power's classification. The grains of HRS appear to be slightly more angular than the latter albeit not clearly at low magnification. In Fig. 6(b) higher magnification is used to estimate the geometrical properties of the constituent grains. A relatively smooth surface is shown by the grains of M31 and Fontainebleau sands, while the grain shape of HRS is characterised by multiple surfaces intersecting at various angles. Similar shape with more pronounced characteristics is evidenced for Longstone and Jamuna sand particles in Fig. 5(b). A quick appraisal of surface texture using the interferometer [21], where an optical view of the sample is converted to an elevation map using interferogram processing, has given the following values for statistical parameters

$$S_a = \frac{1}{m*n}\sum_{ij}\left|Z_{ij}\right| \qquad S_q = \sqrt{\frac{1}{m*n}\sum_{ij}Z_{ij}^2} \qquad (2)$$

[22] shown by Eqs. 2, where m and n are the number of points in the x and y directions, and z is the deviation at each point from the mean height value: Sa=200nm and 30nm and Sq=298nm and 41nm for HRS and M31 respectively, indicating a significant difference between the two sands at grain scale, the grain of M31 sand being very smooth. Surface roughness measurement was made over an area 20x20μm for each particle. Since both sands share the same grading the difference observed in their response to undrained loading can be attributed to grain shape and angularity.

Fontainebleau sand has been described in the literature as a rounded sand [23] while HRS has been described as subangular [24]. In Fig. 7 the response to undrained shear is shown for Fontainebleau sand. As indicated in Table 2 void ratios as well as relative densities of the specimens (FS_1, 2, 3) shown in Fig. 7 are similar to those of the specimens shown in Fig. 3 for HRS and M31 sands respectively. Yet, Fontainebleau sand shows brittle response like M31 sand contrary to HRS which shows stable response. Instability is followed by a quasi-steady state phase that ends at phase transformation points, marked by the broken arrows in Fig. 7(c) at strain levels of 3% to 4% and the specimens regain their strength. This state characterised by moderate deformation was termed [25] quasi-steady as opposed to the conventionally defined steady state [26] which is reached at large shear strains.

The failure envelope, phase transformation and instability lines have been plotted in Fig. 7(a) and the corresponding values for the mobilized angles are $\varphi'=38^0$, $\varphi'_{PTL}=33^0$ and $\varphi'_{IL}=22^0$ respectively, which are very close to the values observed for M31 sand. A denser specimen (FS_4 in Table 2) also included in Fig. 7 shows stable response as observed in Fig. 3(b) for M31 sand previously.

In Fig. 6 the grains of Fontainebleau sand are rounded and relatively smooth which makes them similar to M31 grains hence accounting for the brittle response of the sand. Since Fontainebleau sand is finer than HRS, the difference in their response to undrained shear can be attributed to grain angularity and to a lesser degree to its grading as will also be corroborated by the following Figure 8.

In Fig. 8 the response to undrained torsional shear of the forth uniform sand shown in Fig. 1, the longstone sand (LS) is depicted. The response of LS sand is stable and similar to the response of HRS. The grains of LS sand shown in Fig. 5 are angular. It appears that the shape of the grains is a more prominent factor affecting the response of the sand compared to small variations in grading. Note that LS is finer than HRS while it shows similar response, and finer than Fontainebleau and M31 sands, yet due to the angularity of its grains its behaviour is stable and different than Fontainebleau and M31 sands with rounded grains. Longstone sand which appears to be the most angular of all sands shows higher values for angle of shearing resistance and phase transformation, $\varphi'=41^0$ and $\varphi'=36^0$, respectively for the medium density specimens (LS_1, 2, 3, 4 in Table 2) with relative densities between 39.2% and 40.7% as indicated in Fig. 8(a). The resulting curves of excess pore water pressure and stress-strain are shown in Figs 8(b) and (c) respectively. In the latter phase transformation points have been

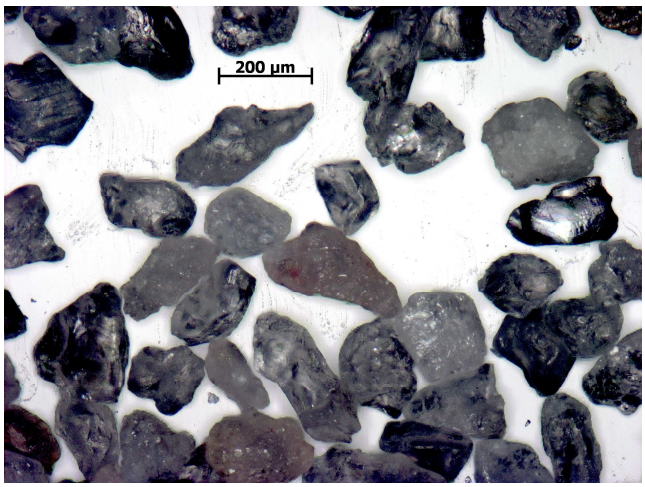

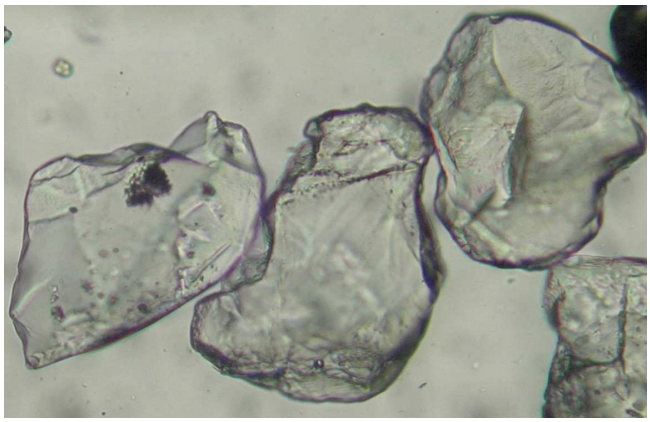

(1) Longstone sand (top)
(2) Jamuna sand (bottom)

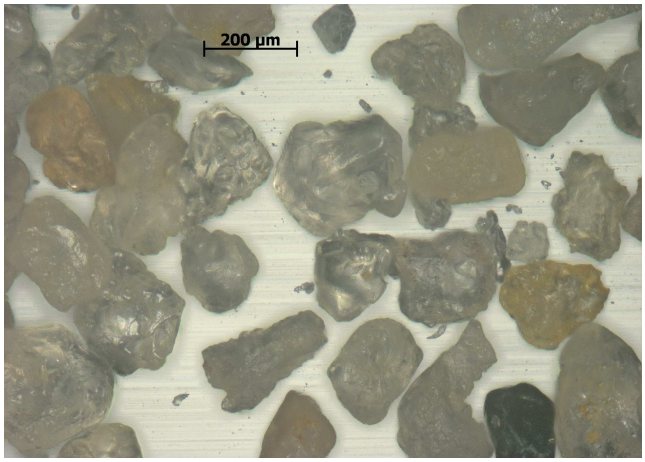

(a)

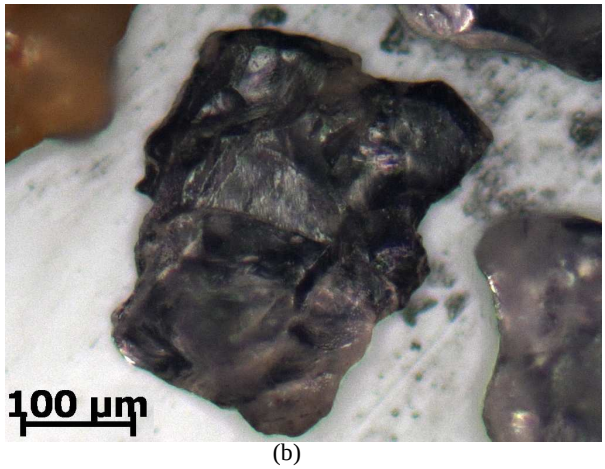

(b)

Roundness classes: Very angular | Angular | Sub-angular | Sub-rounded | Rounded | Well rounded

High Sphericity

Low Sphericity

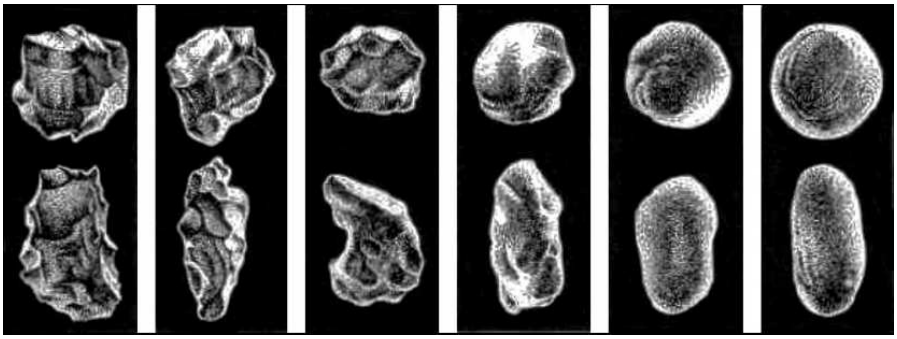

(c)

Figure 5 Visual inspection under the electron scanning microscope for Longstone and Jamuna sand at magnification factors: (a) 50x , (b) 100x and (c) estimation of roundness and shericity adapted from Powers (1953) [20]

marked by arrows. Two denser specimens included in Fig. 8 show higher angle of shearing resistance $\varphi'=43^0$.

However, the effect of grading should not be disregarded. The above comparisons are restricted to uniform, fine, quartz sands with a relatively small variation of their D50. Jamuna sand (JS), has also angular grains as shown in Fig. 5 where grains of JS sand are included. However, its response to undrained triaxial compression is brittle as shown in Fig. 9.

The response of HRS is also shown in this Figure to facilitate comparison with the results of torsional shear tests on HRS shown in Fig. 3. It should be noted that HRS shows stable response whether under torsional shear or triaxial loading in compression (Fig. 9 and Fig. 3) even though the void ratio of the specimens is higher in the triaxial tests. Details of the specimens tested in the triaxial apparatus are shown in Table 3.

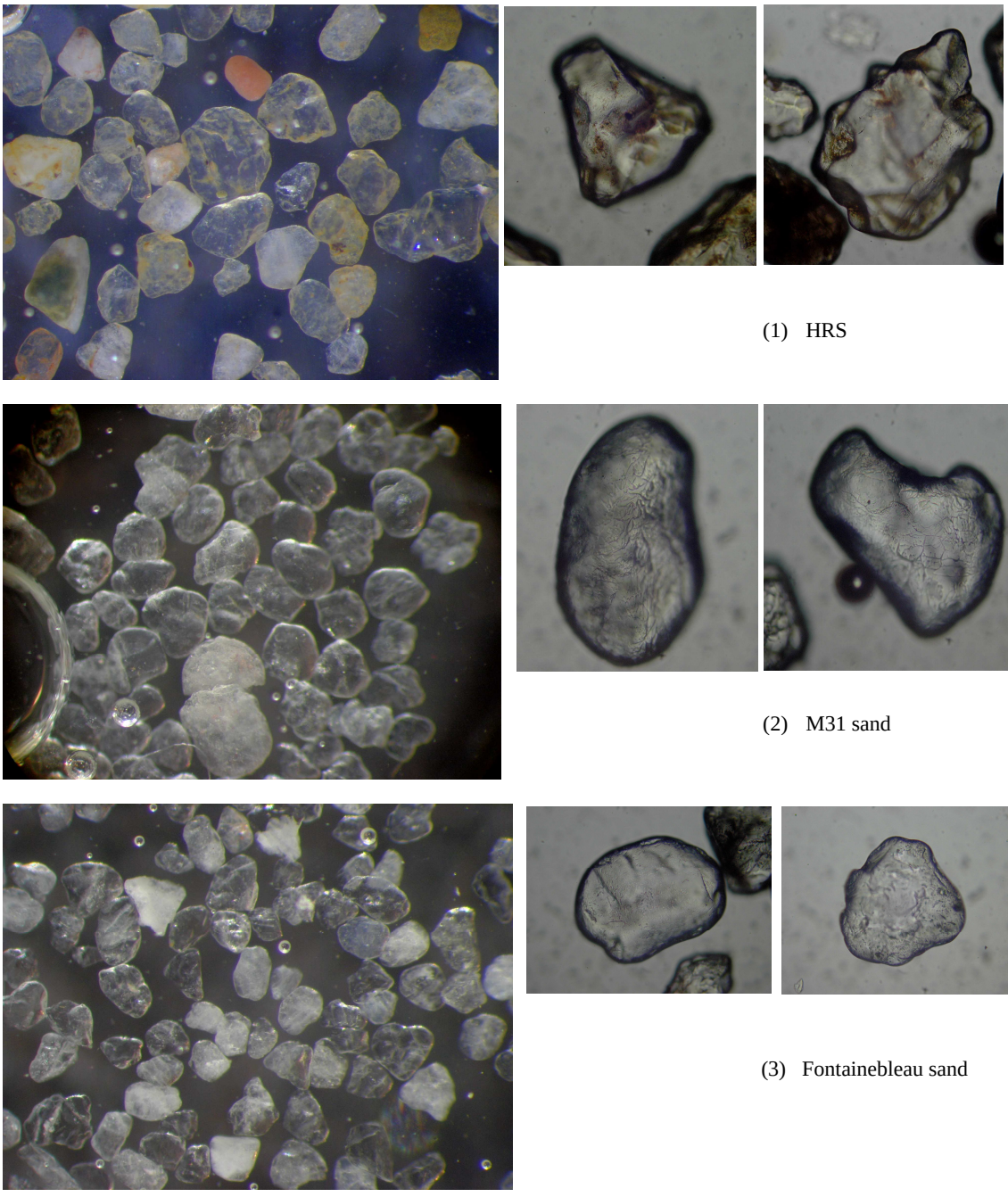

(1) HRS

(2) M31 sand

(3) Fontainebleau sand

(a) (b)

Figure 6 Visual inspection under the electron scanning microscope: (a) magnification factor 50x; (b) 100x. (1) HRS, (2) M31 and (3) Fontainebleau sand

Under triaxial extension loading, also included in Fig. 9, both sands are very weak due to their anisotropic structure ([27], [6], [7]). In Fig. 10 the response of LS sand is shown in undrained triaxial compression for two different loading conditions: strain controlled and stress controlled tests, indicated by the dotted and solid lines respectively.

The latter can be compared with the stress controlled torsional shear tests shown in Fig. 8. Longstone sand in Figs. 8 and 10 shows continuous increase in strength for both loading modes at similar void ratios (Tables 2 & 3). However, under torsional shear the behaviour of LS sand is more contractant than in triaxial compression reflecting its anisotropic structure [28].

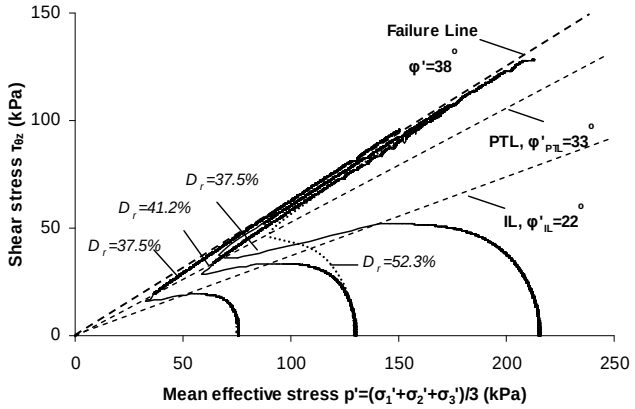

(a)

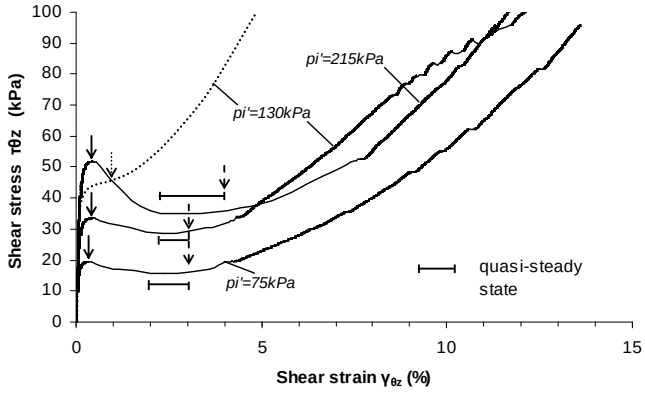

(b)

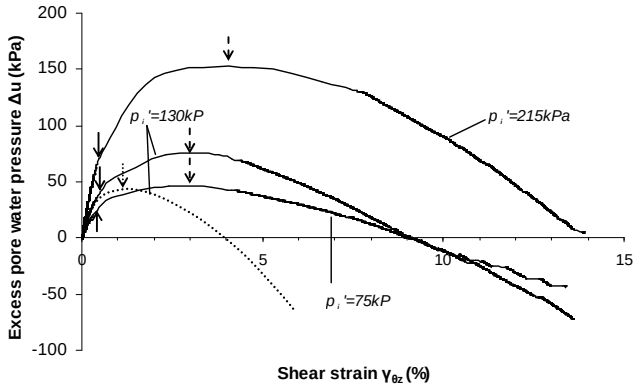

(c)

Figure 7 Undrained torsional hollow cylinder tests for Fontainebleau sand: (a) effective stress paths; (b) stress-strain curves; (c) excess pore water pressure against shear strain curves

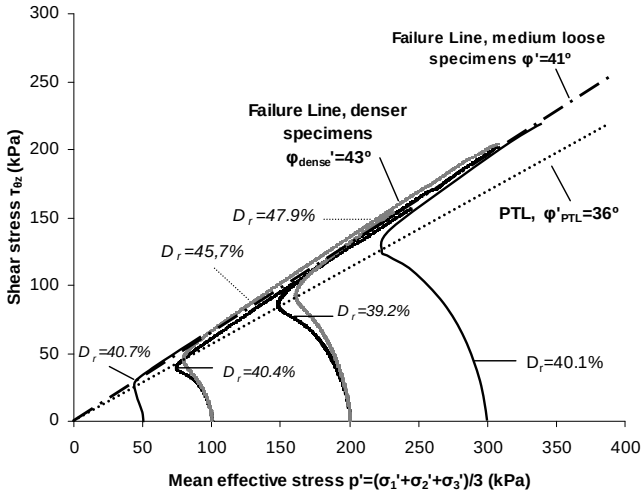

(a)

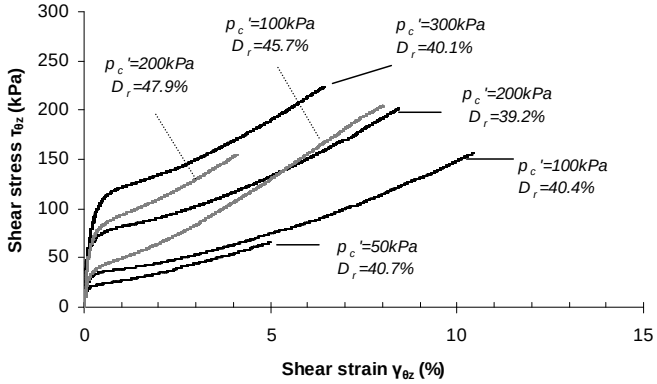

(b)

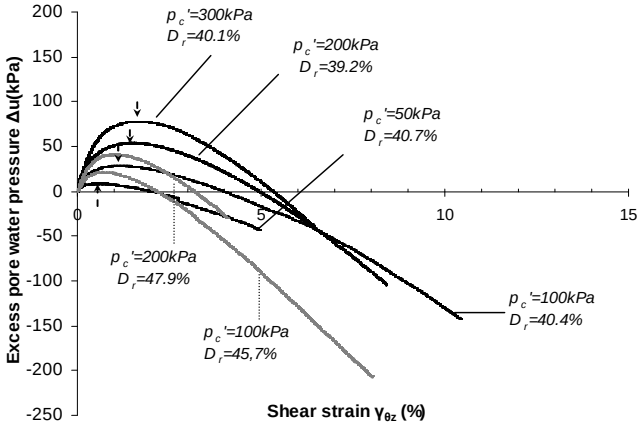

(c)

Figure 8 Undrained torsional hollow cylinder tests for Longstone sand: (a) effective stress paths; (b) stress-strain curves; (c) excess pore water pressure against shear strain curves

Table 2 Specimen characteristics for hollow cylinder tests

Test	Loading Type	e_i	D_r (%)	p_c'(kPa)
HRS_1	TO	0.729	41.0	75
HRS_2	TO	0.735	39.2	130
HRS_3	TO	0.734	39.5	215
HRS_4	TO	0.728	41.3	300
HRS_5	TO	0.668	58.7	130
M31_1	TO	0.733	40.1	75
M31_2	TO	0.731	40.6	130
M31_3	TO	0.733	40.1	215
M31_4	TO	0.611	75.7	100
FS_1	TO	0.743	37.5	75
FS_2	TO	0.731	41.2	130
FS_3	TO	0.743	37.5	215
FS_4	TO	0.695	52.3	130
LS_1	TO	0.840	40.7	50
LS_2	TO	0.841	40.4	100
LS_3	TO	0.846	39.2	200
LS_4	TO	0.842	40.1	300
LS_5	TO	0.821	45.7	100
LS_6	TO	0.813	47.9	200
HRS_6	TX	0.747	35.8	250
HRS_7	TX	0.721	43.3	100
M31_5	TX	0.749	35.4	250
M31_6	TX	0.719	44.2	100
HRS11	TO	0.735	39.2	130
F13	TO	0.732	40.9	130
LS_1AC	TO	0.812	47.3	100
LS_2AC	TO	0.822	43.5	200

TO = torsional shear,
TX = triaxial compression

The strain controlled tests in Fig. 10 can be compared with the response of Jamuna sand (JS) shown in Fig. 9. Although LS and Jamuna sands are both angular the stable behaviour of LS sand contrasts the brittle response of Jamuna sand. If we compare the gradings of the two sands in Fig. 1 we observe that Jamuna sand contains 16% of silt fraction which makes it less uniform than LS, while the sand fraction is similar in both sands (D50~0.15mm), and apparently this is the reason for its brittle behaviour. Lade and Yamamuro (1997) [29] tested two different gradations of Nevada sand, the more uniform consisting of sand sieved between sieve sizes 0.300-0.175mm and the other ranging between 0.300-0.074mm. The two sand gradations were tested under triaxial loading conditions at a relative density of 20%. During loading in compression the more uniform gradation exhibited temporary liquefaction while the wider gradation exhibited complete static liquefaction. The authors inferred that the small size grains in the wider gradation sand may have an effect similar to that of adding fines to a sand, namely increase their liquefaction potential. In Fig. 9 the response of HRS is also shown for comparison. The more uniform HRS is stable. However, the difference in mean diameter

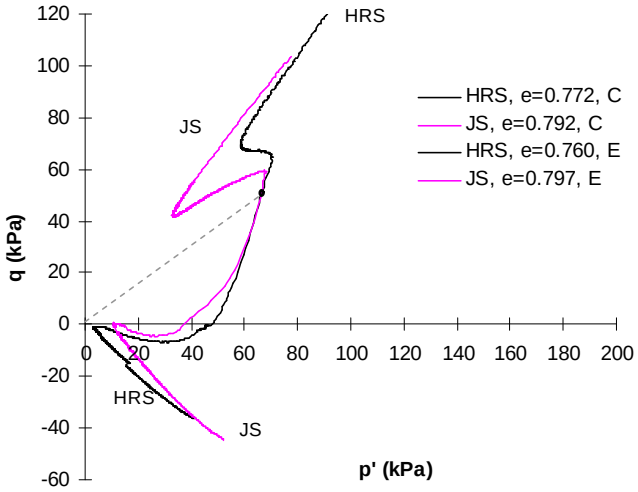

(a)

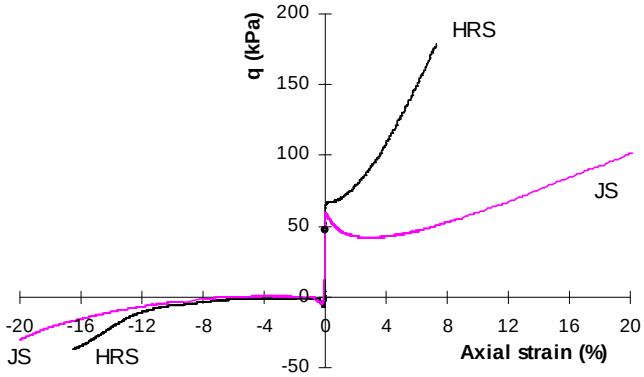

(b)

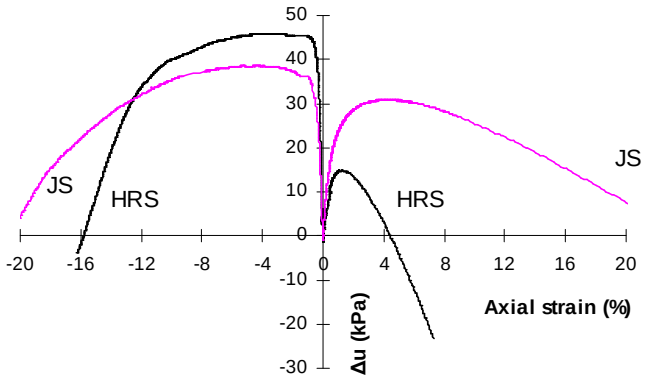

(c)

Figure 9 Triaxial compression and extension tests on anisotropically consolidated loose specimens of HRS and Jamuna sand: (a) effective stress paths; (b) stress-strain curves; (c) excess pore water pressure against axial strain curves

Table 3 Specimen characteristics for triaxial tests

Test	Loading Type	e_i	e_{gi}	p_c'(kPa)
HRS	TX, C	0.772	0.772	75
JS	TX, C	0.792	0.792	75
HRS	TX, E	0.760	0.760	75
JS	TX, E	0.797	0.797	75
LS_7	TX, C	0.843	0.843	500
LS_8	TX, C	0.823	0.823	1000
LS_9	TX, C	0.831	0.831	2000
LS_10	TX, C, L	0.833	0.833	500
LS_11	TX, C, L	0.816	0.816	1000
LS_12	TX, C, L	0.819	0.819	2000
HRS_2.5%HPF4	TX, C	0.761	0.807	75
HRS_2.5%sxm	TX, C	0.746	0.790	75
HRS_2.5%m	TX, C	0.804	0.858	75
HRS_2.5%HPF4	TX, E	0.744	0.788	75
HRS_2.5%sxm	TX, E	0.755	0.800	75
JS_2.5%HPF4	TX, C	0.798	0.844	75
JS_2.5%sxm	TX, C	0.760	0.804	75
JS_2.5%m	TX, C	0.893	0.939	75
JS_2.5%HPF4	TX, E	0.795	0.839	75
JS_2.5%sxm	TX, E	0.767	0.813	75
JS_2.5%m	TX, E	0.895	0.941	75
M31_0%	TX, C	0.790	0.790	100
M31_5%	TX, C	0.790	0.890	100
M31_10%	TX, C	0.780	0.980	100
M31_0%	TX, C	0.590	0.590	100
M31_5%	TX, C	0.610	0.690	100
M31_10%	TX, C	0.660	0.840	100
M31_7	TX, C, L	0.750	0.750	100
M31_8	TX, C, L	0.734	0.734	200
M31_9	TX, C	0.740	0.740	100
M31_10	TX, C	0.732	0.732	200
HRS_8	TX, C, L	0.738	0.738	100
HRS_9	TX, C, L	0.727	0.727	200
HRS_10	TX, C	0.731	0.731	100
HRS_11	TX, C	0.696	0.696	200

TX, C = triaxial compression, strain control
TX, E = triaxial extension, strain control
TX, C, L = triaxial compression, stress control

between HRS and Jamuna sand should be noted, unlike the preceding comparison between LS and Jamuna sand with similar D50 values.

3.2 Effect of small fines contents

The effect of added fines on the behaviour of sands has been addressed in the literature inconclusively. One of the reasons is that the addition of rotund particles (e.g. silt) should be distinguished from that of flat or platy particles of different size (e.g. kaolin, silt or sand-size mica). Moreover, the importance of shape and location of additives in modifying the sand structure is not reflected in measures

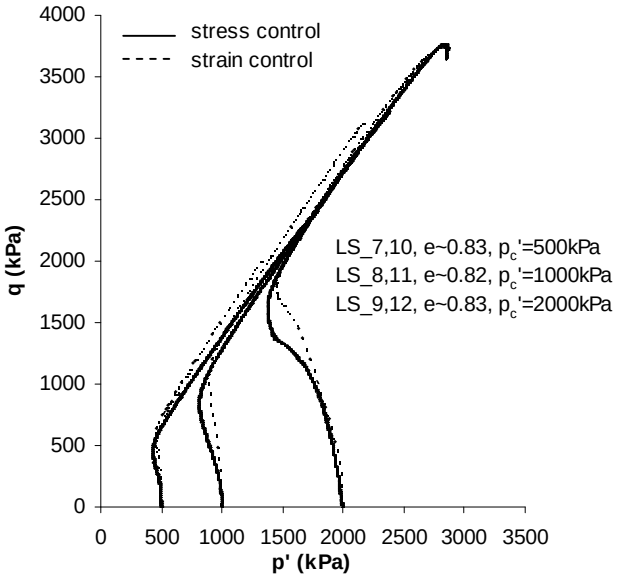

(a)

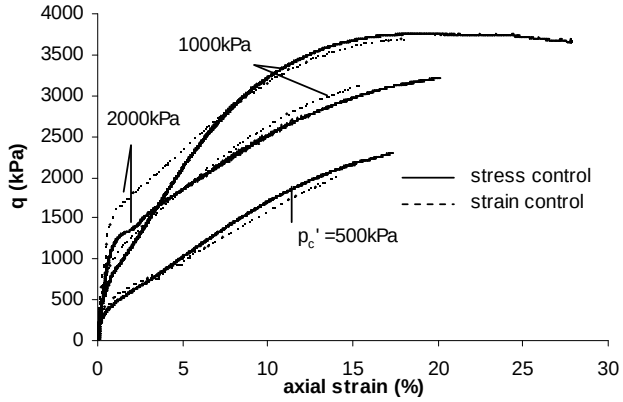

(b)

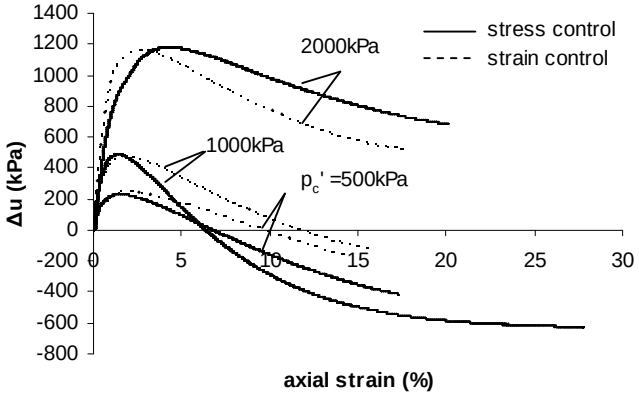

(c)

Figure 10 Triaxial compression stress- and strain-controlled tests on loose specimens of Longstone sand: (a) effective stress paths; (b) stress-strain curves; (c) excess pore water pressure against axial strain curves

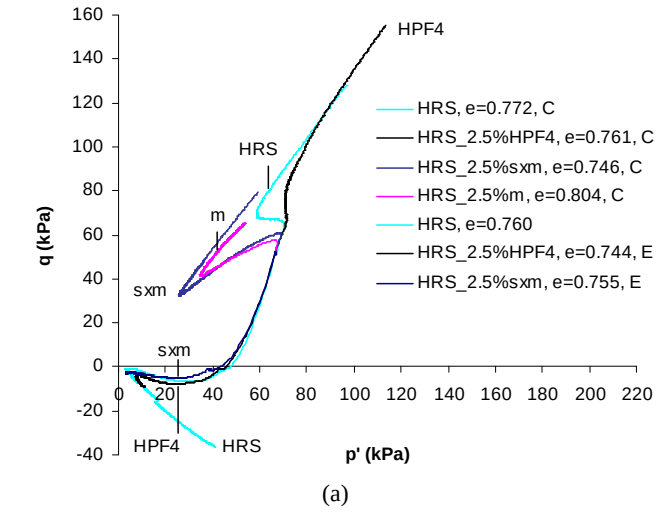

(a)

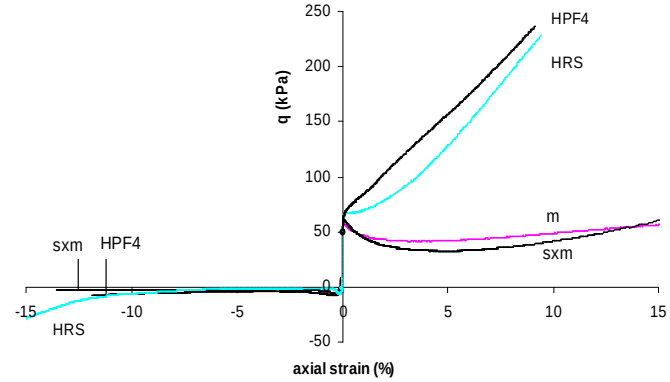

(b)

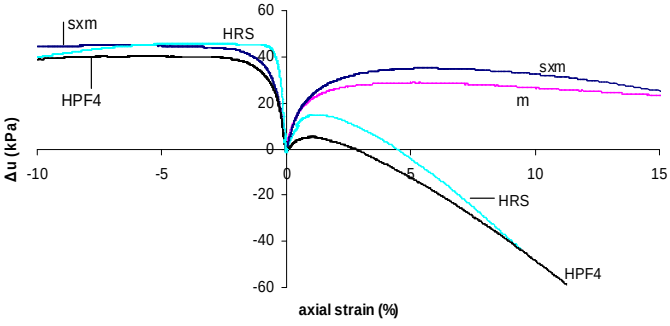

(c)

Figure 11 Triaxial compression and extension tests on anisotropically consolidated mixtures of HRS with additions of 2.5% of various particles: (a) effective stress paths; (b) stress-strain curves; (c) excess pore water pressure against axial strain curves

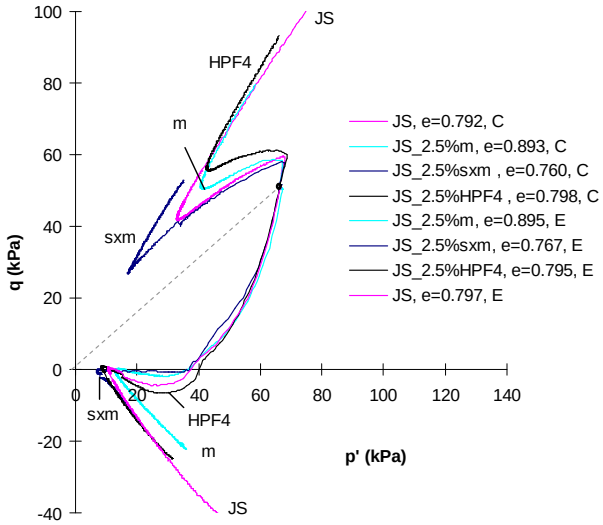

(a)

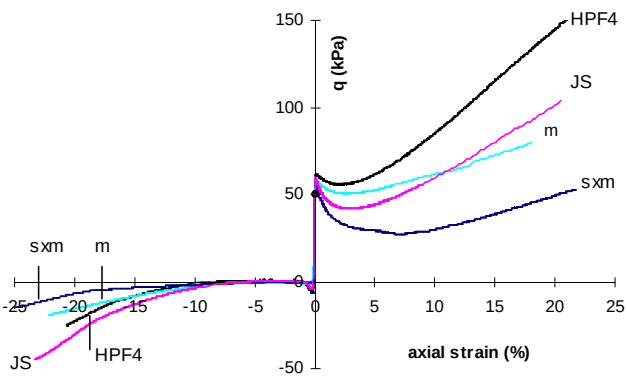

(b)

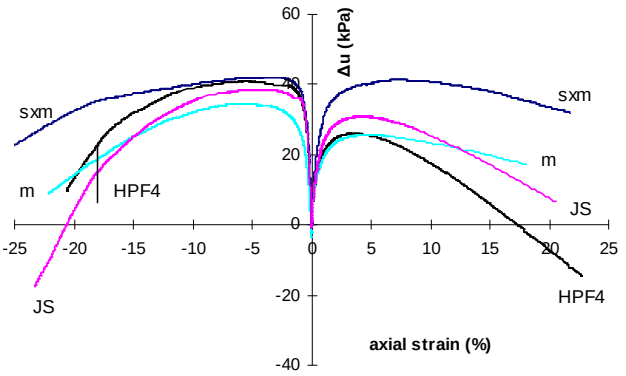

(c)

Figure 12 Triaxial compression and extension tests on anisotropically consolidated mixtures of Jamuna sand with additions of 2.5% of various particles: (a) effective stress paths; (b) stress-strain curves; (c) excess pore water pressure against axial strain curves

such as void ratio or granular void ratio $e_g=(V_v+V_f)/V_s$, where $V_v=V_{voids}$,$V_f=V_{fines}$ and $V_s=V_{sand}$ [30]. Comparisons should be restricted with respect to type of fines, shape and grain characteristics, mineralogy, relative size of coarser (sand) grains and finer grains/particles, relative density of host sand. It should be noted that the above factors affect the response of a sand for the same fines content. At the same granular void ratio, e_g, an increase in fines content would eventually force the coarser sand grains to disperse fully in the finer grain matrix. For fines contents lower than those corresponding to this transition zone the effect of fines content to the observed response of a mixture is examined. The following figures refer to the addition of only small contents of fines. All tests were performed in the triaxial apparatus under strain control in compression and extension. Details of the specimens are shown in Table 3, where initial void ratio and granular void ratio is given.

Fig. 11 shows how the addition of fines at a small content of

only 2.5% by weight can completely alter the behaviour of the host HRS sand. In Fig. 2 the gradings of the added fines are shown. In Fig. 11, in triaxial compression, the non-brittle clean sand exhibits a brittle response when mixed with either sand (m) or silt-size mica (sxm). However, the presence of the same content of silt (HPF4) substantially suppresses the contractive tendencies of the host loose sand resulting in a response similar to that of a denser sand. In triaxial extension the effect of adding 2.5% of fines is small and the loose sand's structure appears to prevail. The effect of the same content of fines on the undrained response of Jamuna sand is examined in Fig. 12.

The addition of 2.5% of sand-size mica (m) has a small effect on stabilizing post peak behaviour contrary to the addition of 2.5% silt-size mica (sxm) that results in a dramatic increase of undrained brittleness in compression and strains to phase transformation. As was the case for HRS, the presence of silt (HPF4) increases transient peak strength and decreases brittleness. In triaxial extension all soils are weak. For both sands the mixture with silt-size mica has the smallest void ratio or granular void ratio yet shows the most unstable response. The nature and distribution of fines play a greater role than void ratio/granular void ratio at least for loose to medium density sand. The ratio of the mean diameter of sand-size mica to

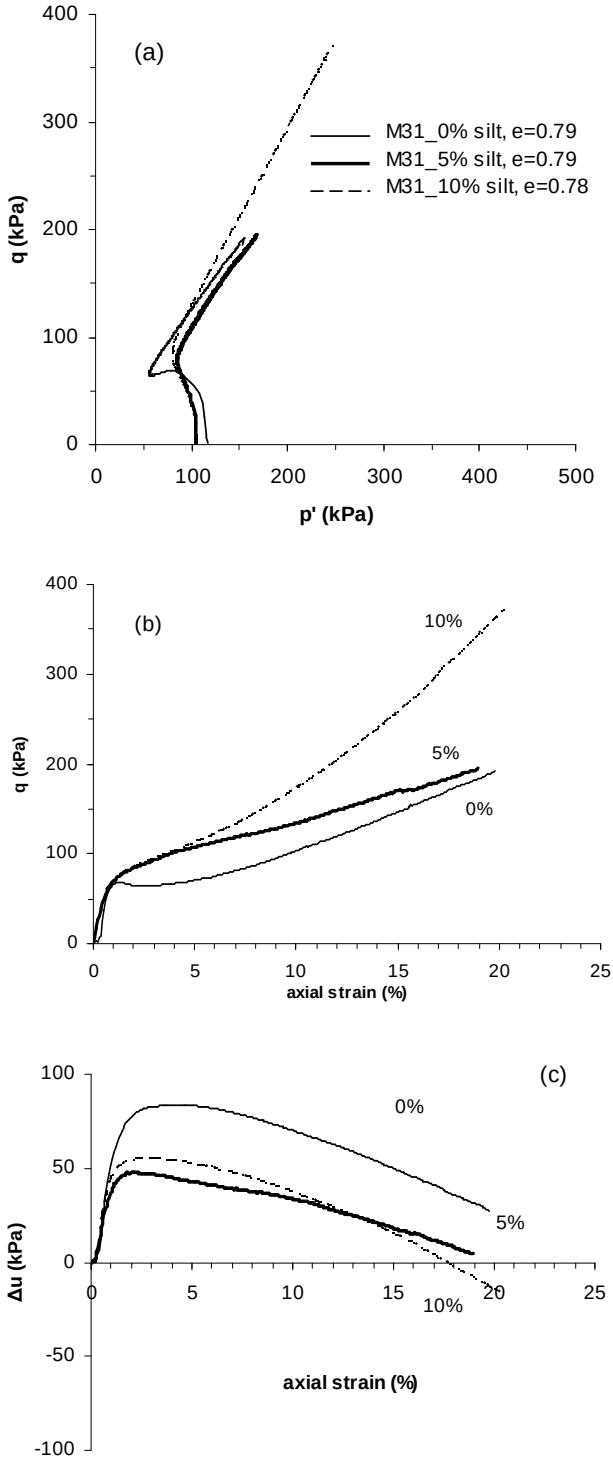

Figure 13 Triaxial compression on loose specimens of M31 sand with additions of 5% and 10% of silt: (a) effective stress paths; (b) stress-strain curves; (c) excess pore water pressure against axial strain curves

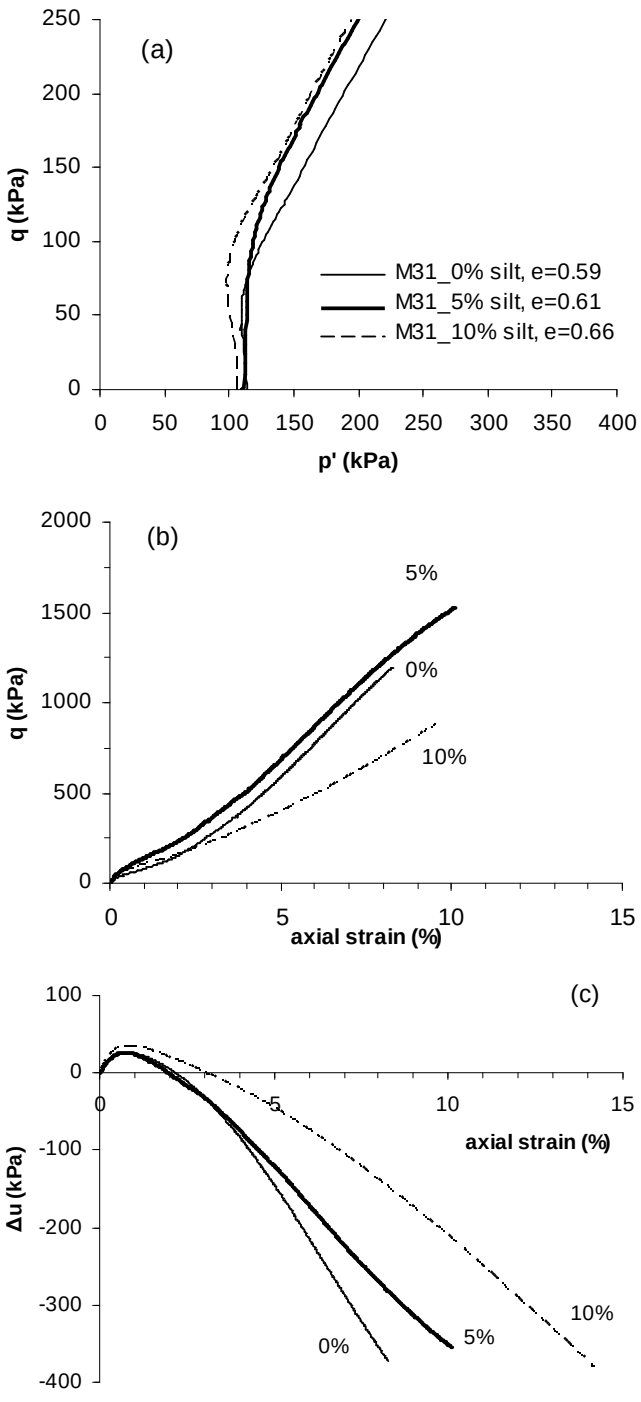

Figure 14 Triaxial compression on dense specimens of M31 sand with additions of 5% and 10% of silt: (a) effective stress paths; (b) stress-strain curves; (c) excess pore water pressure against axial strain curves

that of HRS is about 1 to 3 while it is similar for JS. Hence, its effect is to destabilize HRS while being of similar size slightly increases the strength of Jamuna sand. However, silt-size mica with a mean diameter at least 10 times smaller than the mean diameter of both sands destabilizes them.

On the other hand the round particles of silt being 5 times smaller than both sands' grains may be accommodated between the pores of the sands' structure and increase their strength. This stabilizing effect of silt at small contents has been repeatedly observed in triaxial tests [31] at least for the case of fine sands at the same granular void ratio. Following the preceding discussion related to Figs 11 & 12 the effect of silt would also depend on the relative size of silt to sand particles. However, there is another parameter that could affect the silt function and that is the pore space. The undrained triaxial compression tests shown in Fig. 13 indicate that the presence of silt at relatively low contents appears to result in a decrease in the tendency for contractive response of loose M31 sand.

However, undrained compression tests on dense specimens, shown in Fig. 14, indicate 'reverse' behaviour i.e. the addition of silt does not result in less contractive response compared with clean sand. Yet the effect of the silt is to stabilize the loose sand's response. It should be noted that specimens are compared at similar void ratio hence granular void ratio increasing with fines content.

3.3 Effect of loading conditions

Sand is traditionally considered as a rate independent material. However, sand exhibits substantial creep deformations outside the elastic range, and a time-dependent behaviour may not be negligible. The study of the effects of strain rate on undrained response is outside the scope of this paper. However, in the following tests the effect of two different loading conditions is considered: loading was performed at a constant strain rate of 4% per hour and at a constant rate of load of 2N/min for HRS and M31 sands and 7N/min for Longstone sand tested at higher stresses. These tests were performed in the triaxial apparatus.

In Fig. 15 a comparison is made between the two loading conditions for M31 sand. The void ratios for the triaxial tests on medium density specimens (e=0.750-0.732) M31_7, 8, 9, 10 are included in Table 3. Regarding the effect of loading conditions Fig. 15 shows that under stress control the response of the sand becomes brittle and shear stress drops to a minimum. Subsequently, the sand shows phase transformation, at a higher axial strain compared to the strain controlled tests, followed by dilative tendencies at 5% and 10% axial strain for p'_c=100kPa and 200kPa respectively. Under strain control the behaviour of the sand is stable for e= 0.732-0.740 (M31-9, 10 in Table 3). It is interesting to note that the maximum excess pore water pressure is only slightly affected by the loading conditions in Fig. 15(c). The failure envelope, $\varphi'=30^0$, and the angle at phase transformation, $\varphi'_{PTL}=32^0$ also appear to be unaffected by loading conditions. Similar data are presented in the literature [11], [32]. However, brittleness is introduced under stress control only.

A stress drop in a stress controlled test could be a reflection of the inability of the apparatus to apply the specified stress. It should be noted though that brittleness is observed under both triaxial and torsional stress controlled loading (Figs 15 & 3(b, c, d)) indicating a material property. The specimens did not collapse and showed dilative tendencies. To investigate the effect of the testing system on the material response the results of load cotrolled tests are compared with typical strain controlled tests for specimens of HRS mixed with 7% kaolin at a granular void ratio $e_g=(V_v+V_k)/V_s)=0.800$ (where V_v, V_k and V_s is the volume of voids, kaolin and sand respectively), which display high brittleness even in strain controlled tests. The effective stress at the end of consolidation was 300kPa. The load was applied in steps through a hanger system and was registered through an internal load cell. The records of axial load, axial deformation and pore water pressure were obtained using a UV recorder capable of continuous monitoring.

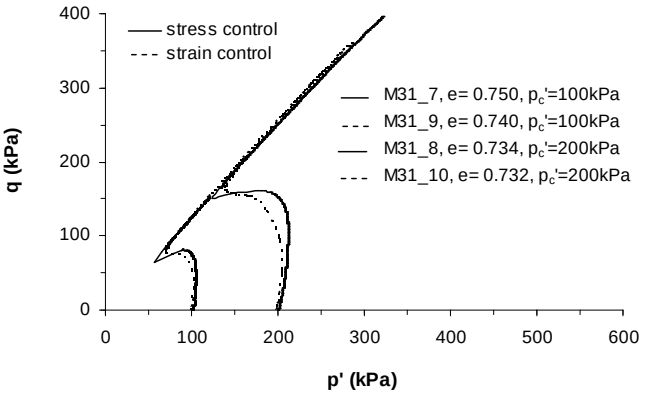

(a)

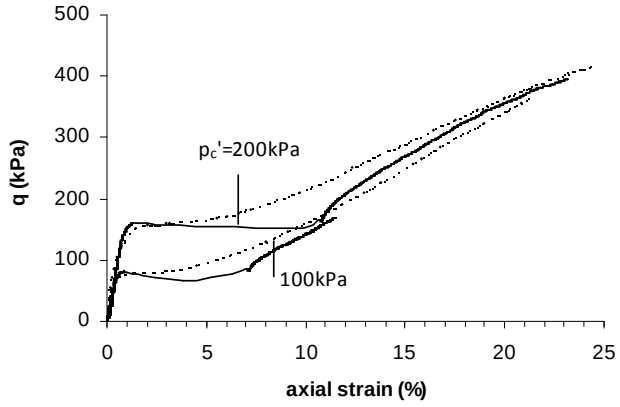

(b)

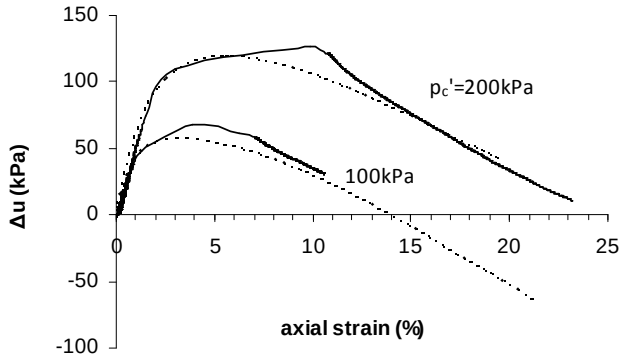

(c)

Figure 15 Triaxial compression stress and strain controlled tests on specimens of M31 sand: (a) effective stress paths; (b) stress-strain curves; (c) excess pore water pressure against axial strain curves

Fig. 16 shows a typical set of results. In the load controlled test once failure occurs, the resistance of the specimen becomes less than the weight of the hanger so that a downward acceleration of the top of the specimen and the loading device takes place. After an axial strain of about 15% the specimen began to dilate and steadily gained strength until it could once again carry the hanger load (point 1 on the failure envelope).

A shift to larger strains at phase transformation, albeit by smaller amounts, is observed during stress controlled loading of sands which show much less tendency for contractive response compared to M31 sand such as the Longstone and HRS sand. The former is shown in Fig. 10, where specimens are tested at higher

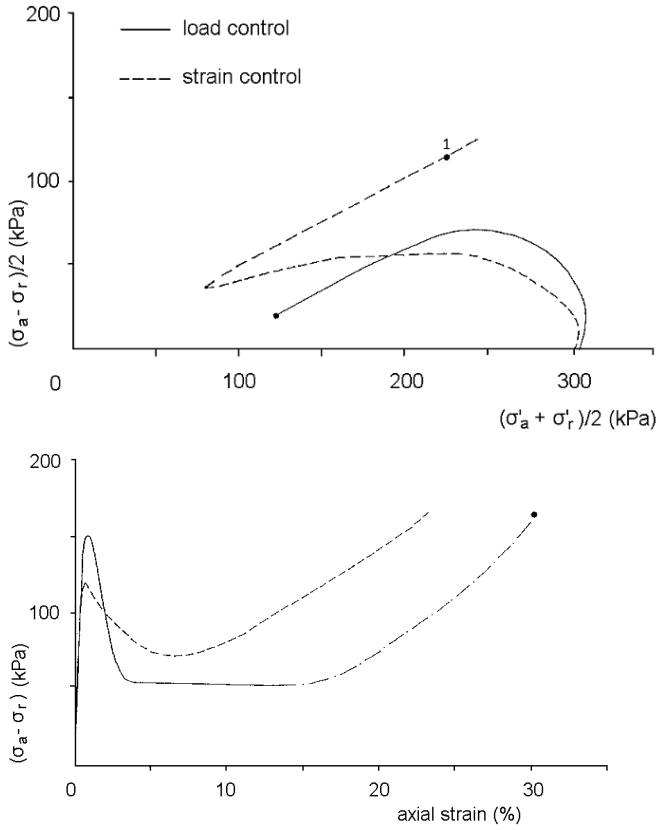

Figure 16 Load and strain control tests on specimens of mixtures of HRS with 7% kaolin (e_g=0.800)

stress levels compared with the tests considered herein, and the latter in Fig. 17. It appears that irrespective of stress level the maximum excess pore water pressure developed during shear is nearly the same for both loading conditions. Similar observations can be made with respect to the failure envelope and phase transformation line. In the low stress range (p'<1000kPa) small differences are observed in the response of LS and HRS to loading conditions in the area where contractive tendencies prevail (increase in excess pore water pressure) while differences arise in the area where dilative tendencies take over. It should be noted that the equivalent strain rate in a stress controlled test varies during loading: being, for the tests reported herein, smaller during the initial (contractive tendencies) stage, soaring to extremely high values if the response of the specimen is brittle, and being similar (M31), smaller (LS) or larger (HRS) in the stage when dilative tendencies take over compared to the constant rate used under strain control. While these data does not resolve the issue the excess pore water pressure after peak appears to be more sensitive to loading conditions (Figs 10(c), 15(c), 17(c)).

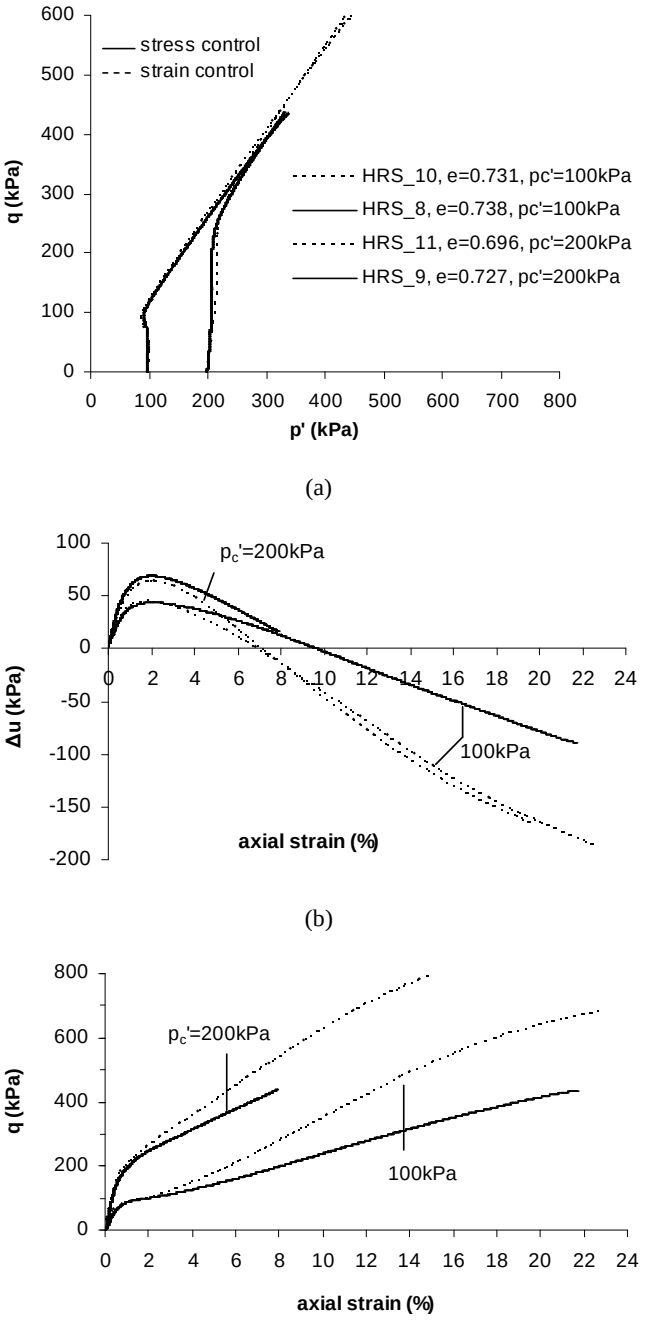

Figure 17 Triaxial compression stress and strain controlled tests on specimens of medium dense HRS: (a) effective stress paths; (b) stress-strain curves; (c) excess pore water pressure against axial strain curves

3.4 Cyclic torsional loading

The response of a sand to cyclic loading is related to its response to monotonic loading ([33], [25], [34], [35], [8]). Two typical cyclic tests are presented in the following figures. In Figs 18 and 19 monotonic and cyclic loading are compared under torsional loading for HRS, showing stable response under monotonic loading, and Fontainebleau sand, showing unstable response under monotonic loading. Fig. 18(a) illustrates the effective stress paths followed by two specimens, included in Table 2, of similar void ratio subjected to monotonic (HRS_2) and cyclic (HRS11) loading, respectively. For the first quarter of the first cycle, between points 1 and 2, the cyclic stress path coincides with the stress path followed under monotonic loading. On unloading to point 3 excess pore water pressure is accumulated and the cyclic stress path moves towards the stress origin. Excess pore water pressure accumulates at a lower rate in the next ten cycles until the effective stress path (point 8) approaches the phase transformation line (PTL) defined under monotonic loading. Symmetrical PTL and failure lines have been plotted in Fig. 18(a). At point 8 shear strain is about 2.5% while just before point 8 the shear strain is only 0.5%, a value similar to that at points 4, 6 and 7 in previous cycles. On unloading and reloading to point 10 the highest rate of excess pore water pressure accumulation is observed and the stress path moves to the origin. Point 10 is a point of phase transformation under cyclic loading, according to Figs 18(c & b) where excess pore water pressure and shear strain

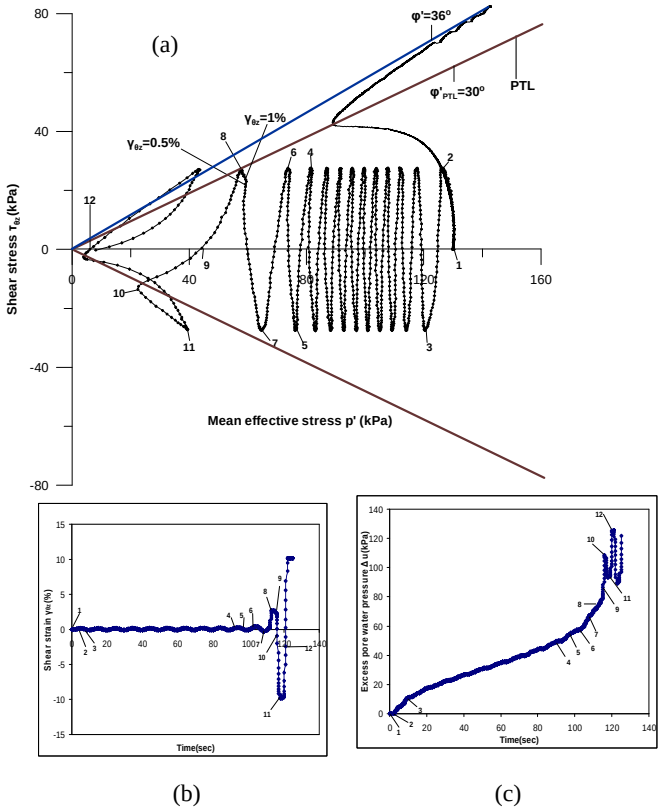

Figure 18 Undrained cyclic torsional hollow cylinder test on HRS: (a) effective stress path; (b) shear strain against time; (c) excess pore water pressure against time

development with time is shown, and appears to lie on the phase transformation line defined under monotonic loading. Point 8 is not a phase transformation point under cyclic loading but is associated with unstable response (sudden increase in shear strain and excess pore water pressure accumulation) which is introduced in the vicinity of the phase transformation line defined under monotonic loading. Once initial liquefaction develops, at the instant the stress cycle passes through the hydrostatic stress state (point 12), a large amount of shear strain is required to mobilize the shearing resistance in the opposite direction (cyclic mobility, [36]). The effective stress ratio mobilized at this stage is the same as that mobilized at large strains along the failure envelope under monotonic loading and is larger than that at phase transformation (φ'=36^0 compared with φ'_{PTL}=30^0).

Fig. 19(a) illustrates the effective stress paths followed by two specimens of Fontainebleau sand at similar void ratio under monotonic and cyclic (FS_2 and F13 in Table 2) torsional loading respectively. The response of Fontainebleau sand under cyclic loading shows common features with HRS during the first and subsequent cycles prior to the introduction of instability, at a shear strain of 0.5% (at point 4) which suddenly increases to 2.2% at point 5 together with a similar increase in pore water pressure and shear strain accumulation as shown in Figs 19(c) and (b) respectively. However, the boundary to stable behaviour appears to be the instability line defined under monotonic loading rather than the phase transformation line observed for HRS. Finally, unloading from stress ratios higher than the ratio at phase transformation, brings the specimens to initial liquefaction (point 11 in Fig. 18 and 7 in Fig. 19). It should be recognized that even at higher density saturated sand can develop pore water pressures when subjected to cyclic loading. The features of behaviour reported herein for medium loose specimens pertain for a wide range of densities, namely: an initial stage related to the first loading cycle, which shows a higher rate of excess pore pressure accumulation than the following steady migration stage, which is related to the number of

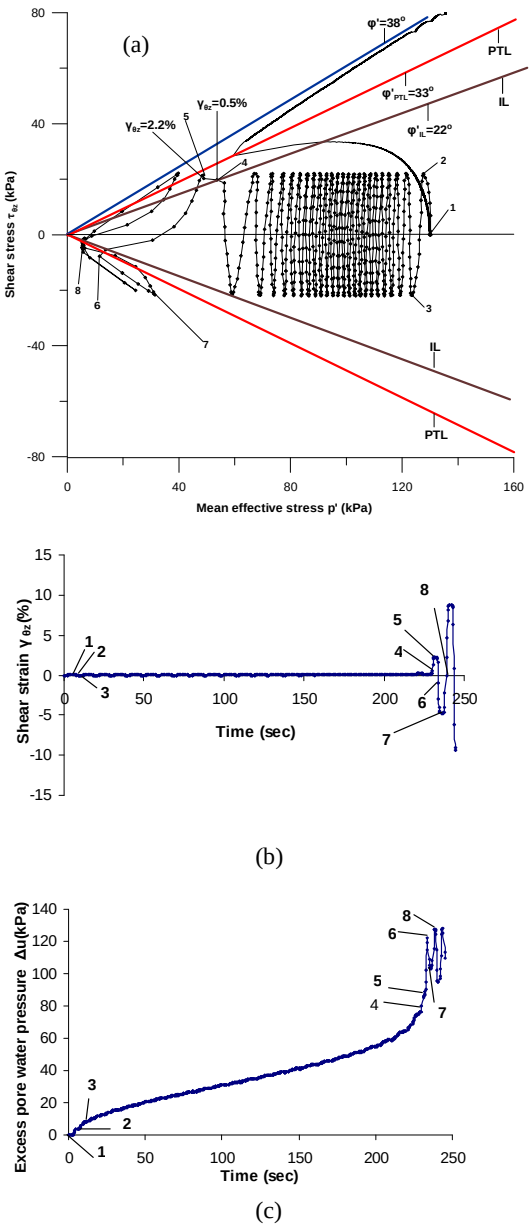

Figure 19 Undrained cyclic torsional hollow cylinder test on Fontainebleau sand: (a) effective stress path; (b) shear strain against time; (c) excess pore water pressure against time

cycles required for the effective stress path to migrate, under undrained loading, close to the phase transformation line (PTL) or the instability line (IL) depending on the behaviour of the material under monotonic loading. Finally, an unstable stage can be identified in the vicinity of the PTL or IL, where large rates of shear strain and excess pore pressure accumulation are observed. The pronounced interrelation of monotonic and cyclic behaviour is associated with the third stage.

3.5 Anisotropic consolidation

In Fig. 20 the undrained response to undrained torsional loading is shown for hollow cylinder specimens of LS sand anisotropically consolidated (LS_1AC, LS_2AC in Table 2). In the same figure the corresponding results of specimens isotropically consolidated to the same effective stress levels (LS_5, LS_6 in Table 2) are included for comparison. Anisotropically consolidated specimens followed initially a constant σ_r' drained path, from a mean effective stress p'=30 kPa, up to the line of constant stress ratio k = σ_r'/σ_a' = 0.5,

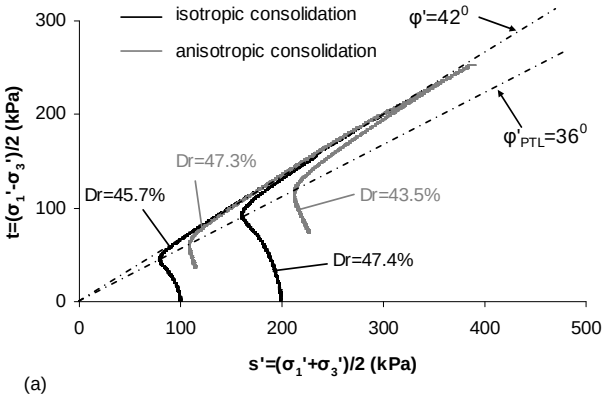

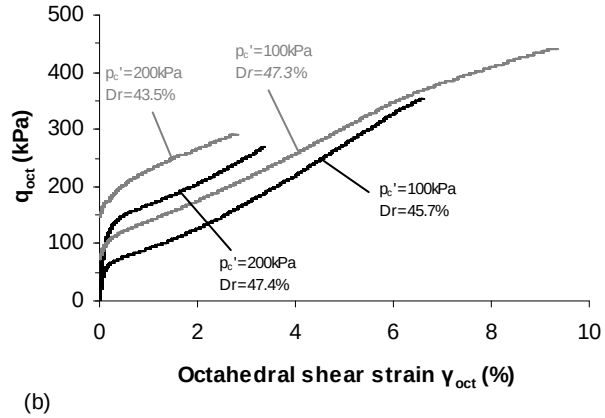

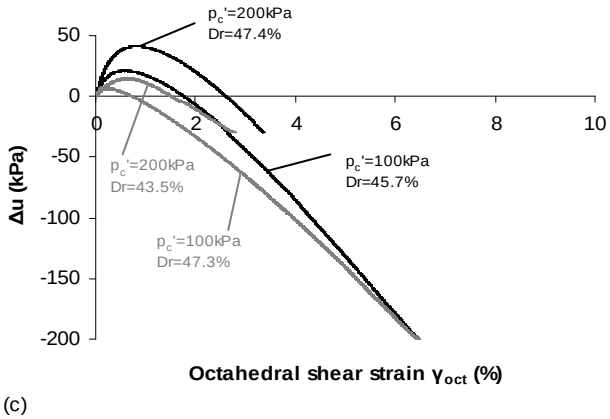

Figure 20 Undrained torsional hollow cylinder tests for isotropically and anisotropically consolidated Longstone sand: (a) effective stress paths; (b) stress-strain curves; (c) excess pore water pressure against shear strain curves

which was subsequently followed to final consolidation stress. After a resting period of 12h torsional shear was applied to the specimens, which resulted to the angle α changing during shear from 0^0 to 25^0 at phase transformation. In Fig. 20(a) the stress paths are shown for the tests in terms of Mohr-Coulomb parameters t and s' in order to observe the effect of anisotropic consolidation on the mobilized angles at phase transformation and failure. It appears that these angles are not affected by anisotropic consolidation. The uniqueness of phase transformation line was reported [37] for two sands irrespective of the angle α or the level of the intermediate principal stress parameter, b. The stress-strain curves in Fig. 20(b) are presented in terms of q_{oct} and γ_{oct} (Eq. 3).

$$q_{oct} = \frac{1}{\sqrt{2}}\left[(\sigma_1-\sigma_2)^2+(\sigma_2-\sigma_3)^2+(\sigma_3-\sigma_1)^2\right]^{\frac{1}{2}}$$
$$\gamma_{oct} = \frac{2}{3}\left[(\varepsilon_1-\varepsilon_2)^2+(\varepsilon_2-\varepsilon_3)^2+(\varepsilon_1-\varepsilon_3)^2\right]^{\frac{1}{2}} \quad (3)$$

The anisotropically consolidated specimens show higher shear stress at similar strains and less tendency to contract in Fig. 20(c), where excess pore water pressure is plotted against shear strain.

4. CONCLUSIONS

This experimental study encompasses monotonic and cyclic response of fine sands in the hollow cylinder and the triaxial apparatus. The behavioural patterns of these sands are compared for identical or similar gradations using the same preparation method, testing techniques and specimen density. Despite these restrictions different response is observed under torsional loading namely, an unstable or brittle response and a stable response with continuous increase in shear stress with torsional loading. The latter has been associated with the angularity of the grains of the sands and to a lesser degree with small variations in grading. It should be noted that the sands were compared at a loose state resulting from water pluviation and as density increases brittleness and contractive tendencies are suppressed. Triaxial tests confirm the above observations.

Larger variations in grading obscure the effect of grain angularity. Jamuna sand with a wider gradation compared to the uniform gradations of the other angular sands shows brittle contrary to stable response under triaxial loading in compression.

Moreover, the role of various additive materials even at small contents (2.5% by weight) in modifying the sand fabric and dramatically changing the undrained behaviour of clean sands is shown when silt-size mica is added to HRS and Jamuna sand. The addition of the same content of sand-size mica introduces instability to HRS and has less influence on Jamuna sand, indicating that the relative size of the fines to the mean grain diameter of the sand might be an important factor for the effect of the added fine. The role of various fines (e.g. platy or rotund) appears to have a pronounced influence on a sand's behaviour and is not reflected in measures such as void ratio or granular void ratio.

Finally, the addition of the same content of silt makes both sands (HRS and JS) more stable in triaxial compression. In triaxial extension the effect of any of the above fines is minimal and the loose sand's response prevails, which is highly anisotropic being much weaker and more contractive in triaxial extension than in triaxial compression. However, the addition of silt in dense M31 sand specimens appears to reverse the behaviour observed for loose M31 sand specimens.

The loading conditions (stress or strain control) affect the post peak stress-strain and excess pore water pressure-strain behaviour of the sands tested herein the effects being larger for the sand with a tendency to unstable or brittle response in triaxial compression.

The behaviour of a sand under cyclic torsional loading appears to be correlated to its response under monotonic loading. HRS with stable response under monotonic loading shows unstable response under undrained cyclic loading in the vicinity of the phase transformation line defined under monotonic loading, while Fontainebleau sand which shows unstable response under monotonic loading shows unstable response under cyclic loading in the vicinity of the instability line defined under monotonic loading.

Under monotonic torsional loading the failure and phase transformation lines do not appear to be affected by the history of consolidation (isotropic or anisotropic) although the response of the sand after consolidation differs.

5. ACKNOWLEDGEMENTS

This research has been co-financed by the European Union (European Social Fund – ESF) and Greek national funds through the Operational Program "Education and Lifelong Learning" of the National Strategic Reference Framework (NSRF) - Research Funding Program: Heracleitus II. Investing in knowledge society through the European Social Fund.

6. REFERENCES

[1] Miura, S. and Toki, S. "Anisotropy in mechanical properties and its simulation of sands sampled from natural deposits", Soils and Foundations, 24, No. 3, 1984, pp69-84.

[2] Lade, P.V. "Initiation of static instability in the submarine Nerlerk berm", Canadian Geotechnical Journal, 30, 1993, pp895-904.

[3] Konrad J.M. and Watts B.D. "Undrained shear strength for liquefaction flow failure analysis", Canadian Geotechnical Journal, 32, 1995, pp783-794.

[4] Sladen, J.A., D'Hollander, R.D., Krahn, J., and Mitchell, D.E. "The liquefaction of sands, a collapse surface approach", Canadian Geotechnical Journal, 22, 1985, pp564-578.

[5] Vaid, Y.P., Chung, E.K.F., and Kuerbis, R.H. "Preshearing and undrained response of sand", Soils and Foundations, 29, No. 4, 1989, pp49–56.

[6] Georgiannou, V.N., Burland, J.B., and Hight, D. W. "The undrained behaviour of clayey sands in triaxial compression and extension", Geotechnique, 41, No.3, 1990, pp383-393.

[7] De Gennaro, V., Canou, J., Dupla, J.C., and Benahmed, N. "Influence of loading path on the undrained behaviour of a medium loose sand", Canadian Geotechnical Journal, 41, 2004, pp166-180.

[8] Georgiannou, V.N. and Tsomokos, A. "Comparison of two fine sands under torsional loading", Canadian Geotechnical Journal, 45, 2008, pp1659-1672.

[9] Sasitharan, S., Robertson, P.K., Sego, D.C., and Morgenstern, N.R. "State-boundary surface for very loose sand and its practical implications", Canadian Geotechnical Journal, 31, 1994, pp321-334.

[10] Chu, J., Leroueil, S., and Leong, W.K. "Unstable behaviour of sand and its implication for slope stability", Canadian Geotechnical Journal, 40, 2003, pp873-885.

[11] Chu, J. & Wanatowski, D. "Effect of loading mode on strain softening and instability behaviour of sand in plane-strain tests", J. Geotech and Geoenv. Engrg, ASCE, 135, 1, 2009, pp108-120.

[12] Kolbuszewski, J.J. "An experimental study of the maximum and minimum porosities of sands", Proc. 2nd ICSMFE, Rotterdam, 1, 1948, pp158-165.

[13] Zdravkovic, L. "The stress-strain-strength anisotropy of a granular medium under general stress conditions", PhD thesis, Imperial College, University of London, 1996.

[14] Georgiannou, V.N., Tsomokos, A. and Stavrou K. "Monotonic and cyclic behaviour of sand under torsional loading", Geotechnique, 58, No. 2, 2008, pp113-124.

[15] Hight, D.W., Gens, A., Symes, M.J. 1983. "The development of a new hollow cylinder apparatus for investigating the effects of principal stress rotation in soils", Geotechnique, 33, No. 4, 1983, pp 355-384.

[16] Bishop, A.W. & Wesley, L.D. (1975). "A hydraulic triaxial apparatus for controlled stress path testing", Geotechnique, 25, No. 4, 1975, pp657-670.

[17] Burland, J.B. & Symes, M.J. "A simple axial displacement gauge for use in the triaxial apparatus", Geotechnique, 32, No. 1, 1982, pp62-65.

[18] Vaid, Y.P., and Negussey D. "Preparation of reconstituted sand specimens", Advanced testing of soil and rock, ASTM, STP977, 1988, pp405-417.

[19] Oda, M., Koishikawa, I., Higuehi, T. "Experimental study of anisotropic shear strength of sand by plane strain test", Soils and Foundations, 18, No. 1, 1978, pp25-38.

[20] Powers, M.C. "A roundness scale for sedimentary particles", Journal of Sedimentary Research, 23, No. 2, pp117-119.

[21] Fogale. "Fogale nanotech user manual", Version 1.5, 2005.

[22] Sacerdotti, F., Griffiths, B., Benati, F. and Kang, H. "The variability of functional and amplitude three-dimensional roughness parameters for electron-beam and electro-discharged textured surfaces", Meas. Sci. Technol., 11, 2000, pp171-177.

[23] Bolton, M.D., Gui, M.W., Garnier, J., Corte, J.F., Bagge, G, Laue, J. and Renzi, R. "Centrifuge cone penetration tests in sand", Geotechnique, 49, No. 4, 1999, pp543-552.

[24] Kuwano, R. and Jardine, R.J. "On measuring creep behaviour in granular materials through triaxial testing", Canadian Geotechnical Journal, 39, 2002, pp1061-1074.

[25] Alarcon-Guzman, A., Leonards, G.A., and Chameau, J.L. 1988. "Undrained monotonic and cyclic strength of sands", J. Geotech. Engrg., ASCE, 114, 10,1988, pp1089-1109.

[26] Poulos, S.J. "The steady state of deformation", J. Geotech. Engrg. Div., ASCE, 107, No. 5, 1981, pp553-562.

[27] Vaid, Y.P. and Thomas, J. "Liquefaction and postliquefaction behaniour of sand", Journal of Geotechnical Engineering, 121, No. 2, 1995, pp163-173.

[28] Tsomokos, A.and Georgiannou, V.N. "Effect of grain shape and angularity on the undrained response of fine sands", Canadian Geotechnical Journal, 47, 2010, pp539-551.

[29] Lade, P.V. & Yamamuro, J.A. "Effects of nonplastic fines on static liquefaction of sands", Canadian Geotechnical Journal, 34, 1997, pp918-928.

[30] Georgiannou, V.N. "The undrained response of sands with additions of particles of various shapes and sizes", Geotechnique, 56, No. 9, 2006, pp639-649.

[31] Papadopoulou, A. and Tika, Th. "The effect of fines on critical state and liquefaction resistance characteristics of non-plastic silty sands", Soils and Foundations, 48, No. 5, 2008, pp713-725.

[32] Been, K., Jefferies, M.G., and Hachey, J. "The critical state of sands", Geotechnique, 41, No. 3, 1991, pp365-381.

[33] Symes, M.P.R., Gens, A., and Hight, D.W. "Undrained anisotropy and principal stress rotation in saturated sand", Geotehnique, 34, No. 1, 1984, pp1-27.

[34] Shibuya, S., Hight, D.W., and Jardine, R.J. "Four-dimensional local boundary surface of an isotropically consolidated loose sand", Soils and Foundations, 43, No. 2, 2003, pp89-103.

[35] Shibuya, S. and Hight, D. W. "A bounding surface for granular material", Soils and Foundations, 27, No.4, 1987, pp123-136.

[36] Seed, H.B., and Lee, K.L. "Liquefaction of saturated sands during cyclic loading", J. Soil Mech. Fdn Div., ASCE, 92, No. 6, 1966, pp105-134.

[37] Uthayakumar, M., and Vaid, Y.P. "Static liquefaction of sands under multiaxial loading", Canadian Geotechnical Journal, 35, No. 2, 1998, pp273-283.